

Supplementary Information for

First principles selection and design of mid-IR nonlinear optical halide crystals

By Lei Kang, David Muñoz Ramo, Zheshuai Lin*, Paul D. Bristowe*, Jingui Qin*, and Chuangtian Chen

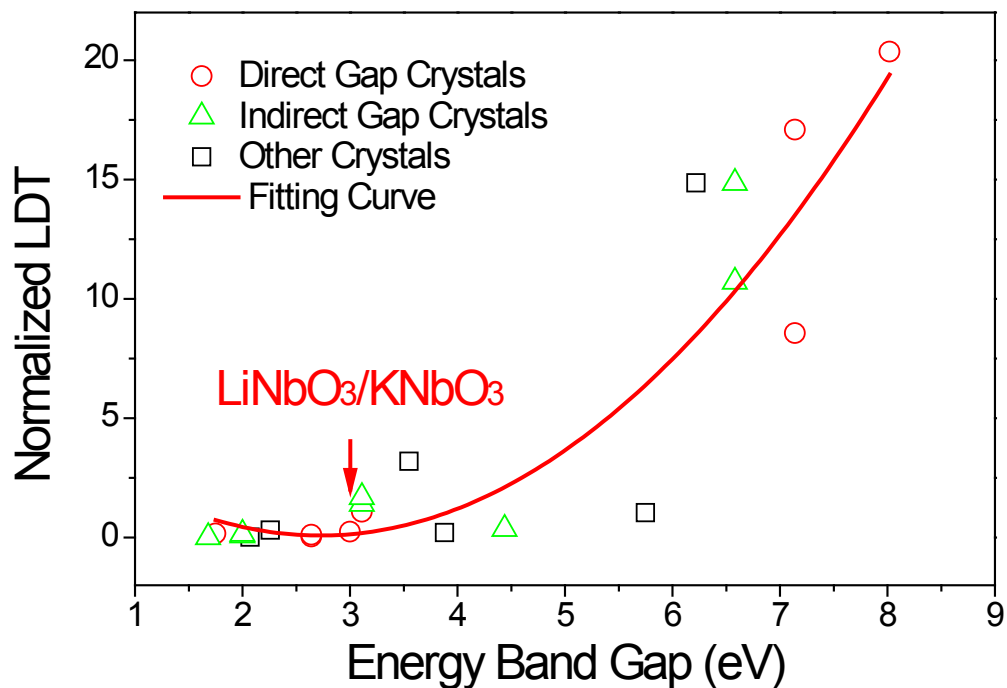
Table of Contents

1. Table S1: Experimental transparent window, SHG coefficients, energy band gaps and corresponding laser damage thresholds in typical NLO crystals.
2. Fig. S1: Tendency curve showing the relationship between laser damage thresholds and energy band gaps in typical NLO crystals.
3. Formula S1: Formula for calculating the theoretical output powers and the conversion efficiencies in the non-depleted pump approximation.
4. Fig. S2: Lone pairs of electrons located at Sb^{3+} atoms in (a) $\text{NaSb}_3\text{F}_{10}$ and (b) SbF_3 described by the electron-localization-function (ELF) method.
5. Table S2: Crystallographic data of the crystals studied including CsGeX_3 , $\text{Cs}_2\text{Hg}_3\text{X}_8$, $\text{NaSb}_3\text{X}_{10}$ and SbX_3 ($X = \text{F}, \text{Cl}, \text{Br}, \text{I}$).
6. Fig. S3 Electronic band structures of the representative halides CsGeX_3 ($X = \text{Cl}, \text{Br}, \text{I}$), CsCdBr_3 , $\text{Cs}_2\text{Hg}_3\text{I}_8$, SbF_3 , $\text{NaSb}_3\text{F}_{10}$, and HgBr_2 .
7. Fig. S4: Charge density distribution in the equatorial plane of the $[\text{GeX}_6]$ octahedron in (a) CsGeCl_3 ; (b) CsGeBr_3 ; (c) CsGeI_3 and of the $[\text{NbO}_6]$ octahedron in (d) KNbO_3 .
8. Fig. S5: Energy band gap E_g and SHG effect d_{ij} as a function of halide anion X .
9. Fig. S6: Discussion of the kinetic stability of the designed crystal $\text{Cs}_2\text{Hg}_3\text{Cl}_8$ using the calculated phonon spectrum.
10. References

1. Table S1 Experimental transparent window, SHG coefficients, energy band gaps and laser damage thresholds (LDT) in typical NLO crystals. The symbols “D” and “I” in parentheses in the fourth column indicate whether the energy band gap of crystal is direct or indirect. In order to make the measured LDT values at the different wavelengths (λ) and laser pulse times (τ_p) comparable, the LDT values are shown normalized in the last column. The normalization uses the fact that the LDT is roughly proportional to the ratio between the wavelength and the square root of the pulse time, i.e., $\lambda/\sqrt{\tau}$. The optical properties come from Ref. [1], while the direct/indirect nature of the energy band gaps comes from Ref. [2-13]

| Samples | UV to IR window (μm) | SHG at 1064 nm | Band gaps (eV) | LDT (MW/cm ²) at specific (λ/nm ; τ_p/ns) | Normalized LDT |
|---|-----------------------------------|----------------|----------------|--|-----------------------|
| LiB ₃ O ₅ | 0.155~3.2 | $d_{32}=0.85$ | 8.02(D) | 19000 (1064nm; 1.3ns) >900 (1064nm; 9ns) | 20.36 >2.54 |
| KB ₅ O ₈ ·4H ₂ O | 0.162~1.5 | $d_{33}=0.05$ | 7.67 | >85 (1064nm; 12ns) >43 (266nm; 8ns) | >0.28 >0.46 |
| KH ₂ PO ₄ | 0.174~1.57 | $d_{36}=0.39$ | 7.14(D) | 18000 (1053nm; 1ns) 8000 (1064nm; 1.3ns) 5000 (1064nm; 1ns) | 17.09 8.57 4.70 |
| β -BaB ₂ O ₄ | 0.189~3.5 | $d_{22}=2.3$ | 6.58(I) | 10000 (1064nm; 1.3ns) 5000 (1064nm; 10ns) | 10.72 14.86 |
| CO(NH ₂) ₂ | 0.2~1.43 | $d_{36}=1.17$ | 6.22 | 5000 (1064nm; 10ns) | 14.86 |
| CsH ₂ AsO ₄ | 0.216~1.87 | $d_{36}=0.4$ | 5.75 | 350 (1064nm; 10ns) | 1.04 |
| LiIO ₃ | 0.28~6 | $d_{33}=4.5$ | 4.44(I) | 120 (1064nm; 10ns) | 0.36 |
| HIO ₃ | 0.32~2.3 | $d_{14}=6$ | 3.88 | 55 (530nm; 15ns) | 0.20 |
| KTiOPO ₄ | 0.35~4.5 | $d_{33}=10.7$ | 3.55 | 2000~3000 (1064nm; 11ns) 30000 (526nm; 0.03ns) | 6.23~9.35 9.88 |
| KTiOAsO ₄ | 0.35~5.3 | $d_{33}=16.2$ | 3.55 | >1200 (1064nm; 8ns) | >3.19 |
| LiNbO ₃ | 0.4~5.5 | $d_{33}=27$ | 3.11(D) | 150 (694nm; 25ns) | 1.08 |
| KNbO ₃ | 0.4~4 | $d_{33}=20.6$ | 3.11(I) | 150~180 (532nm; 25ns) | 1.41~1.69 |
| LiInS ₂ | 0.41~12 | $d_{33}=16$ | 3.00(D) | 67 (1064nm; 15ns) | 0.24 |
| AgGaS ₂ | 0.47~13 | $d_{36}=12.5$ | 2.64(D) | 20 (1064nm; 15ns) 10 (1064nm; 20ns) 35 (1064nm; 12ns) | 0.07 0.04 0.11 |
| HgGa ₂ S ₄ | 0.55~13 | $d_{36}=24$ | 2.26 | 60 (1064nm; 30ns) | 0.31 |
| Ag ₃ AsS ₃ | 0.6~13 | $d_{22}=16.6$ | 2.07 | 3 (1064nm; 14ns) | 0.01 |
| GaSe | 0.62~20 | $d_{22}=54$ | 2.00(I) | 30 (1064nm; 10ns) | 0.09 |
| HgS | 0.62~13 | $d_{11}=50$ | 2.00(I) | 40 (1064nm; 17ns) | 0.16 |
| AgGaSe ₂ | 0.71~19 | $d_{36}=33$ | 1.75(D) | 30 (1064nm; 35ns) | 0.17 |
| ZnGeP ₂ | 0.74~12 | $d_{36}=75$ | 1.68(I) | 3 (1064nm; 10ns) | 0.01 |

2. **Fig. S1** Tendency curve showing how the normalized LDT and energy band gap is related for the NLO crystals given in Table S1. It is found that if the normalized LDT of a NLO crystal is required to be higher than 1.0 (corresponding to about 100 MW/cm^2 for a nanosecond laser which is enough for almost all academic and commercial purposes), the energy band gap should be larger than that of $\text{LiNbO}_3/\text{KNbO}_3$ ($\sim 3\text{eV}$) as indicated by the red arrow. There is no obvious causal relation between the LDT values and whether the energy band gap is direct or indirect in these crystals.



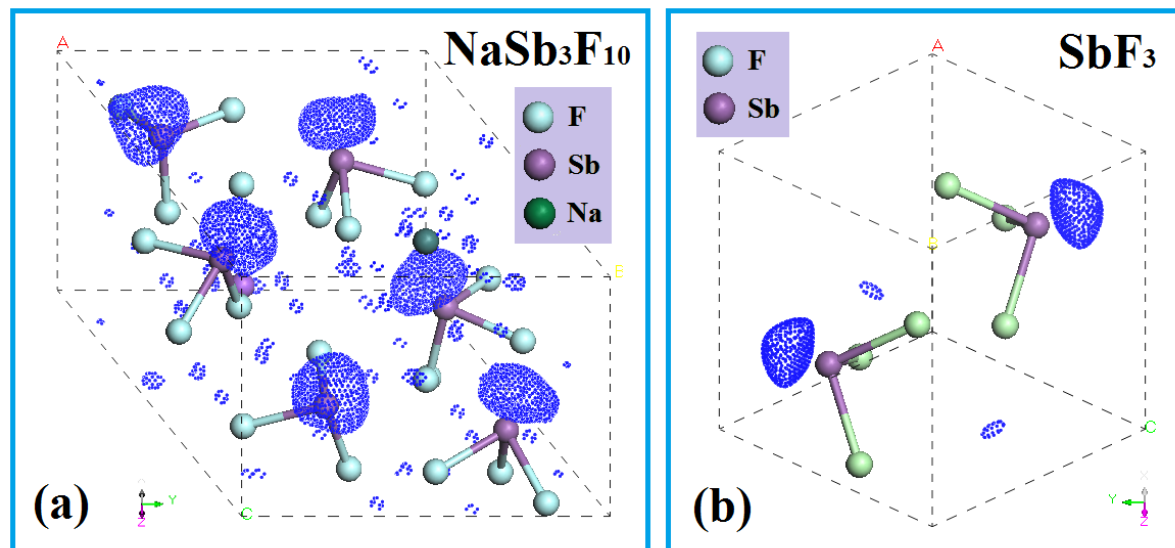
3. Formula S1 In the non-depleted pump approximation, the second harmonic output conversion efficiency η is given by the following expression if the phase-matching condition is satisfied [14]:

$$\eta = \frac{P_2}{P_1} = \frac{2\pi^2 d_{eff}^2 L^2 P_1}{\epsilon_0 c n_1^2 n_2 \lambda_2^2 A}$$

where d_{eff} is the effective SHG coefficient of the crystal in the phase-matching direction, L is the optical path in the crystal, ϵ_0 is the vacuum permittivity; c is the speed of light in vacuo, n_i is refractive index of the light with wavelength λ_i , $A=\pi\omega_0^2$ is the sectional surface area of the laser with radius ω_0 , and P_i is the corresponding power of the λ_i -beams.

From the above formula, it is clear that in order to keep the efficiency η unchanged for second harmonic generation in a crystal, the ratio between d_{eff} and wavelength λ_2 should be fixed. Therefore, d_{eff} would be 10 times larger in the IR region ($\lambda \sim 2000$ nm) than in the UV region ($\lambda \sim 200$ nm) in order to obtain the same conversion efficiency. Since KDP is usually used as the standard NLO crystal in the UV region, the SHG effect d_{eff} in a good IR NLO crystal should be $10 \times d_{eff}(\text{KDP})$.

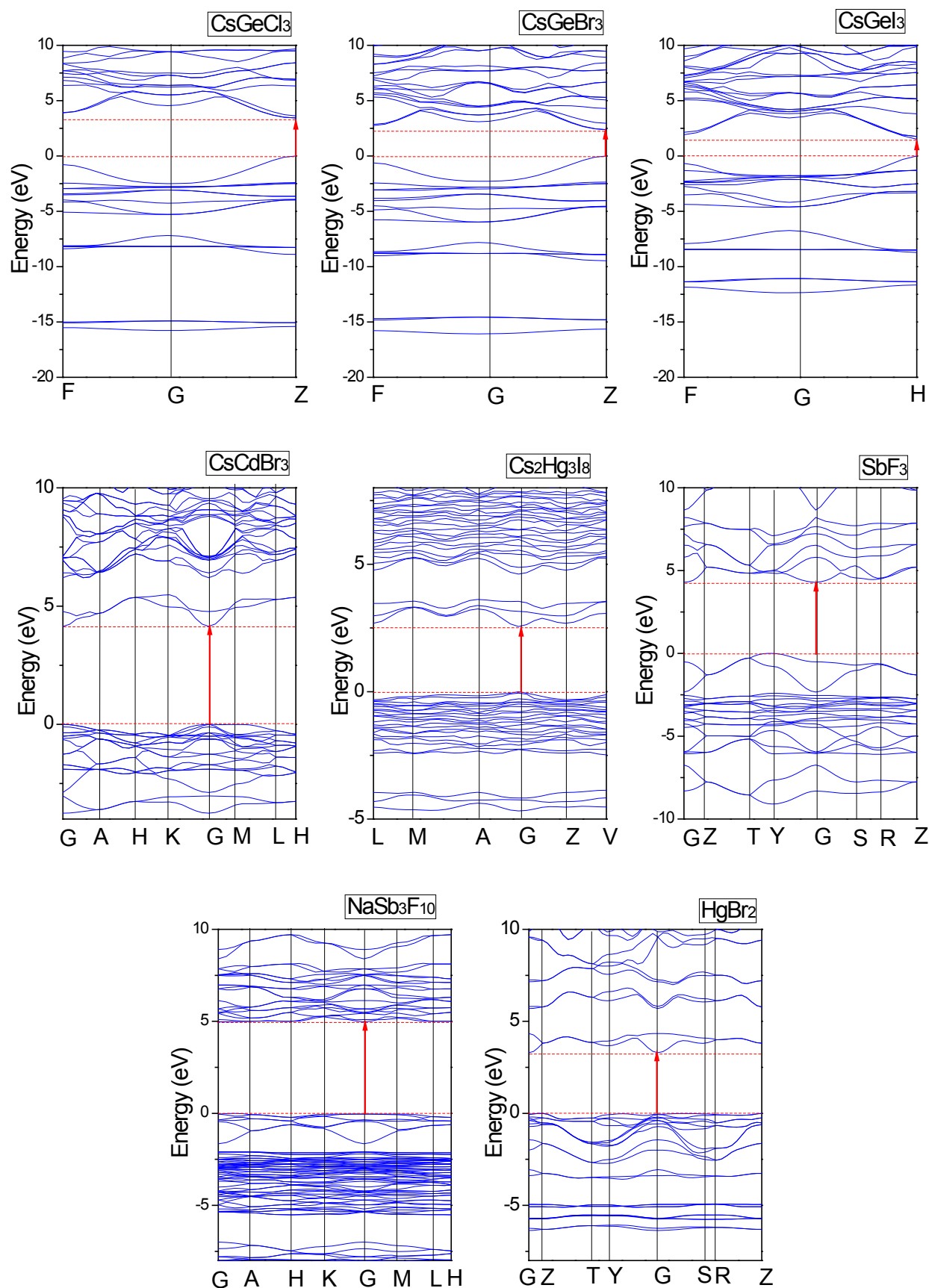
4. **Fig. S2** The stereoactive lone electron pairs located at Sb^{3+} atoms in (a) $\text{NaSb}_3\text{F}_{10}$ and (b) SbF_3 described using the electron-localization-function (ELF) method^[15].



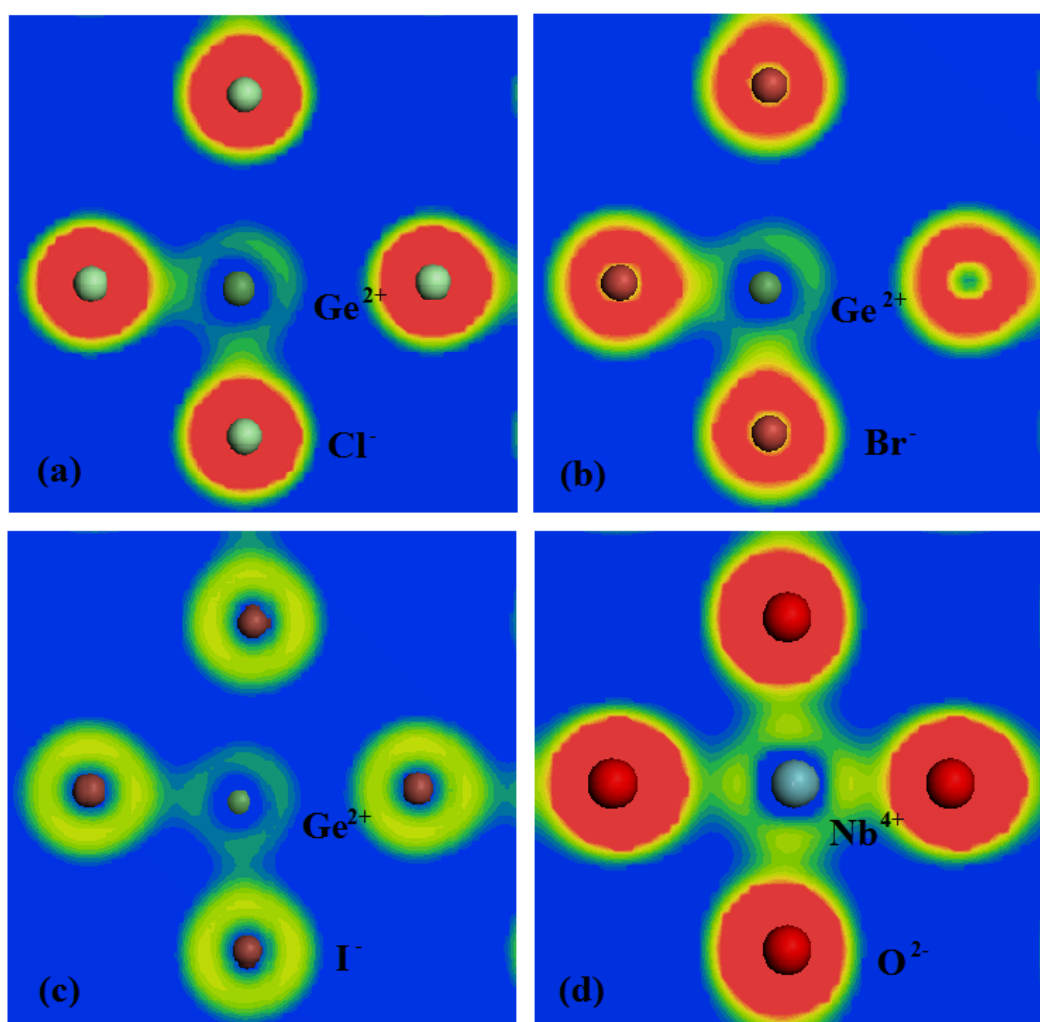
5. Table S2 Calculated and experimental crystallographic data of the crystals studied including CsGeX_3 , $\text{Cs}_2\text{Hg}_3\text{X}_8$, $\text{NaSb}_3\text{X}_{10}$ and SbX_3 ($X = \text{F}, \text{Cl}, \text{Br}, \text{I}$). The star * represents hypothetical crystal. The values in parentheses are the experimental data.

| | Crystal System | Space Group | a (Å) | b (Å) | c (Å) | α (deg) | β (deg) | γ (deg) | Unit Volume (\AA^3) | | | |
|---------------------------------------|--------------------------------|-----------------|----------------|-----------------|----------------|-------------------|------------------|--------------------|-----------------------------------|--|--|--|
| CsGeF_3^* | Rhombohedral-Centred Hexagonal | R3m | 4.60 | | | 94.07 | | | 96.57 | | | |
| CsGeCl_3 | | R3m | 5.13 (5.43) | | | 90.06 (89.72) | | | 135.03 (160.45) | | | |
| CsGeBr_3 | | R3 | 5.14 (5.44) | | | 90.05 (89.63) | | | 135.80 (161.34) | | | |
| CsGeI_3 | | R3m | 5.68 (5.98) | | | 90.00 (88.61) | | | 183.71 (213.98) | | | |
| $\text{Cs}_2\text{Hg}_3\text{Cl}_8^*$ | Centered Monoclinic | C1m1 | 6.16 | 19.52 | 6.55 | 90 | 106.23 | 90 | 755.40 | | | |
| $\text{Cs}_2\text{Hg}_3\text{Br}_8^*$ | | | 6.59 | 19.96 | 6.91 | 90 | 108.43 | 90 | 863.07 | | | |
| $\text{Cs}_2\text{Hg}_3\text{I}_8$ | | | 7.19 (7.43) | 21.29 (21.7) | 7.43 (7.68) | 90 (90) | 109.73 (108) | 90 (90) | (1177.65) | | | |
| $\text{NaSb}_3\text{F}_{10}$ | Primitive Hexagonal | P6 ₃ | 8.20 (8.29) | | | 90 | 120 | | 431.45 (451.78) | | | |
| $\text{NaSb}_3\text{Cl}_{10}^*$ | | | 9.92 | | | | | | 763.04 | | | |
| $\text{NaSb}_3\text{Br}_{10}^*$ | | | 10.48 | | | | | | 907.83 | | | |
| $\text{NaSb}_3\text{I}_{10}^*$ | | | 11.39 | | | | | | 1174.72 | | | |
| SbF_3 | C-Centered Orthorhombic | Cmm2 | 4.43 (4.48) | | | 90 | 67.89 (67.13) | 132.76 (134.05) | | | | |
| SbCl_3^* | | | 5.55 | | | 90 | | 240.42 | | | | |
| SbBr_3^* | | | 5.86 | | | 90 | 64.98 | 280.50 | | | | |
| SbI_3^* | | | 6.63 | | | 90 | 63.25 | 352.42 | | | | |

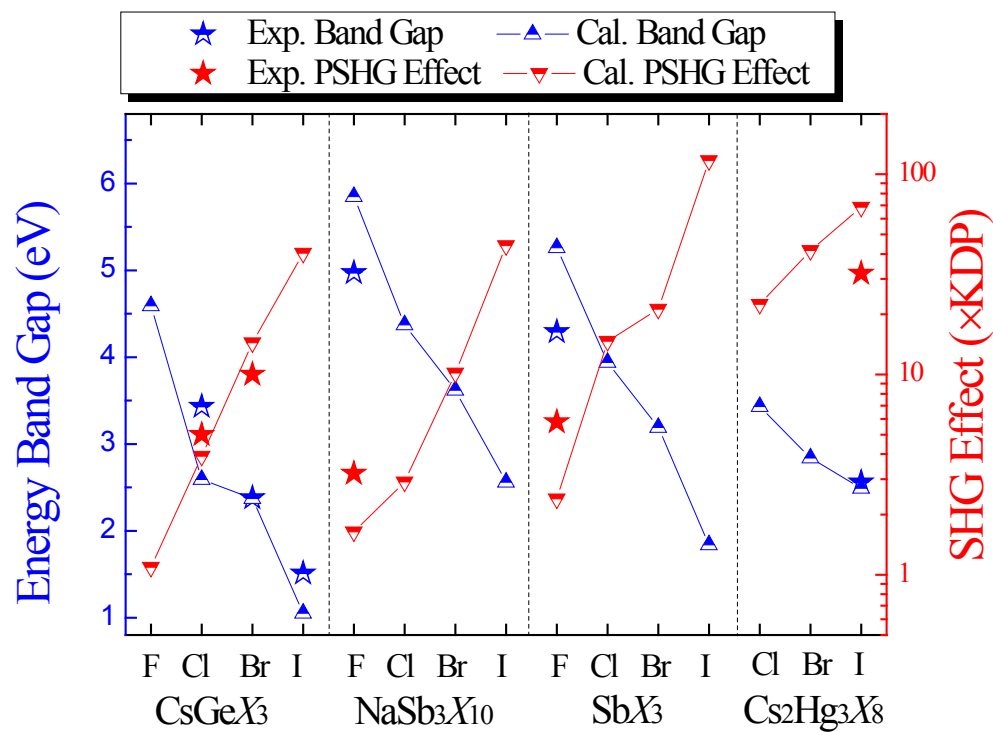
6. **Fig. S3** Electronic band structures of the representative halides $\text{CsGe}X_3$ ($X = \text{Cl}, \text{Br}, \text{I}$), CsCdBr_3 , $\text{Cs}_2\text{Hg}_3\text{I}_8$, SbF_3 , $\text{NaSb}_3\text{F}_{10}$, and HgBr_2 .



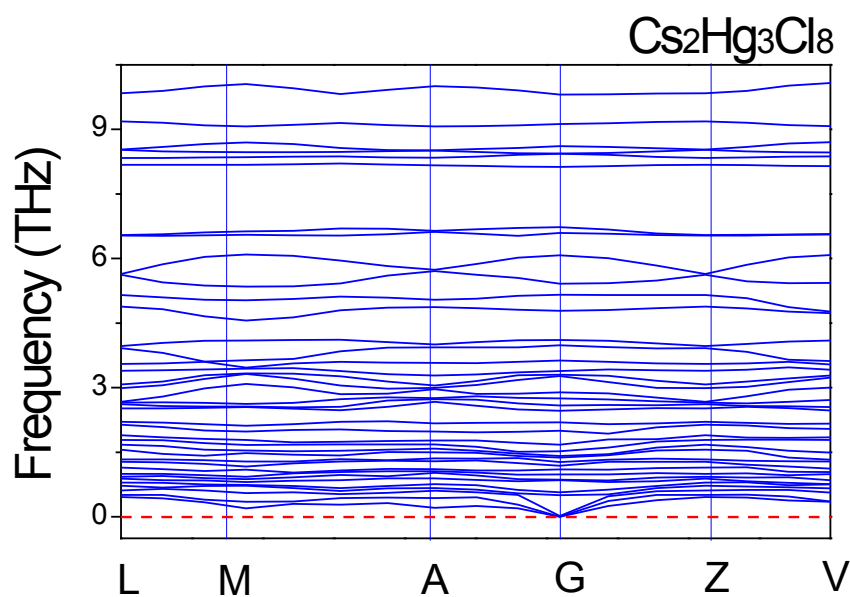
7. **Fig. S4** Charge density distribution in the equatorial plane of the $[GeX_6]$ octahedron in (a) $CsGeCl_3$; (b) $CsGeBr_3$; (c) $CsGeI_3$, and of the $[NbO_6]$ octahedron in (d) $KNbO_3$. It is clear that the electron density distribution in the $[NbO_6]$ octahedron is much more delocalized than that in $[GeX_6]$ octahedron. So the optical response anisotropy to the incident radiation, i.e., optical birefringence, in $KNbO_3$ is larger than that in $CsGeX_3$. Red is high density, blue is low density.



8. **Fig. S5** The energy band gap E_g and SHG effect d_{ij} as the halide anion X varies from F to Cl, Br, and I, from which the descending tendency of E_g and the ascending tendency of d_{ij} are clearly seen.



9. **Fig. S6** Phonon spectrum of the hypothetical halide crystal $\text{Cs}_2\text{Hg}_3\text{Cl}_8$ calculated from density functional theory. None of the imaginary phonon modes are observed, revealing that this crystal is kinetically stable. In the first-principles calculations (using CASTEP), the linear response method is used together with q-point meshes spanning less than $0.03/\text{\AA}^3$ for the dispersion of phonon properties. This method for investigating structural stability was also adopted previously by Yao^[16], Sheng^[17] and the present authors^[18]



10. References

- [1] V. G. Dmitriev, G. G. Gurzadyan and D. N. Nikogosyan, Handbook of nonlinear optical crystals. 3nd Edition, Springer Press, 1999.
- [2] Z. S. Lin, J. Lin, Z. Z. Wang, C. T. Chen, *Phys. Rev. B*, **2000**, 62 (3), 1757-1764.
- [3] Z. S. Lin, Z. Z. Wang, C. T. Chen, M. -H. Lee, *J. Chem. Phys.* 2003, 118, 2349-2356.
- [4] J. Lin, M. -H. Lee, Z. -P. Liu, C. T. Chen, C. J. Pickard, *Phys. Rev. B* **1999**, 60 (19), 13380-13389.
- [5] G. Yao, Y. Chen, X. -Y. An, Z. -Q. Jiang, L. -H. Cao, W. -D. Wu, Y. Zhao, *Chinese Physics Letters*, 30, 067101.
- [6] W. Y. Ching, Z. -Q. Gu, Y. -N. Xu, *Phys. Rev. B* 1994, 50, 1992-1995.
- [7] S. Cabuk, Optoelectronics and Advanced Materials-Rapid Communications, 2007, 1 (3) 100-107.
- [8] T. -H. Ma, C. -H. Yang, Y. Xie, L. Sun, W. -Q. Lv, R. Wang, C. -Q. Zhu, M. Wang, *Comp. Mater. Sci.* 2009, 47, 99-105.
- [9] S. Laksari, A. Chahed, N. Abbouni, O. Benhelal, B. Abbar, *Comp. Mater. Sci.* 2006, 38, 223-230.
- [10] A. V. Kosobutsky, S. Yu. Sarkisov, V. N. Brudnyi, *J. Phys. Chem. Solids*, 2013, 74, 1240-1248.
- [11] S. -R. Sun, Y. -H. Dong, *Solid State Commun.* 2006, 138, 476-479.
- [12] A. Chahed, O. Benhelal, S. Laksari, B. Abbar, B. Bouhafs, N. Amrane, *Physica B* 2005, 367, 142-151.
- [13] V. N. Brudnyi, V. G. Voevodin, S. N. Grinyaev, *Phys. Solid State*, 2006, 48 (11), 2069-2083.
- [14] Richard L. Sutherland, *Handbook of Nonlinear Optics* (1996) vol. 36 Marcel Dekker, Inc.,.
- [15] A. D. Becke and K. E. Edgecombe, *J. Chem. Phys.* **1990**, 92 (9), 5397-5403.
- [16] Y. Yao, et al. *Phys. Rev. Lett.* **2009**, 102, 229601.
- [17] X. -L. Sheng, Q. -B. Yan, F. Ye, Q. -R. Zheng, and G. Su, *Phys. Rev. Lett.* **2011**, 106, 155703.
- [18] L. Kang, Z. S. Lin, J. G. Qin, and C. T. Chen, *Sci. Rep.* **2013**, 3, 1366.